

## NEIGHBORHOOD-BASED ALGORITHM TO FACILITATE THE REDUCTION OF SKIN REFLECTIONS IN RADAR-BASED MICROWAVE IMAGING

B. Maklad, C. Curtis, E. Fear<sup>\*</sup>, and G. Messier

Department of Electrical Engineering, Schulich School of Engineering, University of Calgary, Calgary, AB Canada T2N 1N4, Canada

**Abstract**—Radar-based microwave imaging is being investigated as a complementary diagnostic tool for breast cancer detection. One of the major challenges associated with radar-based breast imaging is the removal of the overwhelming reflection caused by the skin. This paper presents an algorithm that has been designed for realistic 3D scenarios. The algorithm is tested on a variety of realistic 3D numerical breast models, as well as measured data from a phantom and patient. In all cases, the reflections from the skin are significantly reduced, facilitating detection of known tumors.

### 1. INTRODUCTION

Radar-based microwave imaging has been proposed as a complementary approach for breast imaging [1–3]. This technique involves illuminating the breast with a pulse that is short in time (ultra-wideband in frequency) using an appropriate antenna. In a monostatic system, the antenna is typically scanned around the breast, recording reflections at a number of physical locations [4, 5]. At all antenna positions, a dominant reflection is received from the skin due to the differences in the properties of the skin compared to the interior and exterior of the breast. The skin reflections must be reduced at each antenna prior to investigation of reflections arising from the breast interior. The ensuing reflections are then analyzed in order to identify the presence and location of scattering objects in the breast interior, such as any tumors present.

---

*Received 22 December 2011, Accepted 24 February 2012, Scheduled 2 March 2012*

<sup>\*</sup> Corresponding author: Elise C. Fear (fear@ucalgary.ca).

Several methods have been proposed to reduce the reflection from the skin (termed skin subtraction algorithms). The majority of the proposed techniques involve estimating the skin response at each antenna with a combination of signals received at other antennas, then subtracting the estimate from the target signal. In [6], the Woody averaging algorithm is employed to approximate the skin response as an average of the time shifted and scaled signals recorded as the antenna is scanned around the model (i.e., at the same vertical location). Results for this technique have been reported for 3D cylindrical and hemispherical numerical breast models. This technique is improved upon in [3], where a recursive least squares (RLS) technique is applied to more effectively reduce the early time response. This involves calculating filter coefficients to match the candidate signals to the target for each time sample. The Woody averaging method is applied to the later time responses, and the two signals are finally concatenated. This method has primarily been tested on cylindrical breast phantoms. In [7], the RLS method is also employed to reduce early-time reflections in measured and simulated data collected from cylindrical phantoms. Clustering is used in order to select similar responses to include in filtering; however, limited details of this selection are provided. Finally, Bond et al. proposed a technique that estimates the skin response in the target signal using a filtered combination of the signals recorded at all other antennas [2]. Using adaptive signal processing theory, the estimate is optimized over the initial segment of the signal, which is assumed to be dominated by the skin response. This approach has been proven to be effective on data simulated using realistic 2 dimensional (2D) models. In [8], the technique proposed in [2] was modified in order to be applicable to multi-static data and has been tested on realistic 2D numerical breast models.

Several other approaches have been explored to reduce the response from the skin without relying on filtered combinations of reflections recorded at a selection of antennas. The first of these is a frequency domain approach which involves modeling the frequency response of the system and eliminating poles of the response corresponding to the skin reflection [9]. While promising results were obtained when tested on 3D computational models, criteria for determining the poles corresponding to the skin response must be identified. As the test cases do not appear to include significant clutter, it is not clear whether this algorithm is robust to more realistic cases. In [10], a windowing approach is introduced to remove the skin response, incorporating an entropy criterion to define the window length. Again, initial test results appear promising; however it is not

clear if the windowing approach provides reasonable results in realistic scenarios where the skin responses overlap other reflections in the model. Finally, a multi-static system uses the differences between two data sets to reduce the skin reflections [5]. In this case, antennas are distributed over a hemispherical surface and the hemisphere is rotated slightly between measurements.

To date, none of the approaches aimed at reducing the skin reflection in monostatic systems have been tested on measured or simulated signals collected from 3D models with realistic shapes. Reports of work with 3D models simply subtract the skin response recorded from a model consisting of a skin layer bounding a homogenous medium [11]. Therefore, a robust approach to reducing skin reflections from 3D models of the breast is required. This is a challenging task for several reasons. First, the curvature, thickness and properties of the skin may vary over the breast. This implies that the skin reflections change as the antenna is scanned to various locations around the breast. Second, variations in the properties of the breast interior are expected due to the presence of multiple tissues (fat, glandular and fibrous tissues). As the skin reflection contains contributions from the boundary between the skin and exterior of the breast, as well as the skin and interior of the breast, differences in skin signals recorded at various locations are expected. This was noted for the 2D case in [1].

In this paper, we describe a skin subtraction method that estimates the skin response at a given antenna as a filtered combination of the skin reflections measured at neighboring antennas. The proposed method enhances the algorithm reported in [2] by selecting a physically and characteristically relevant neighborhood of antennas to estimate each skin response. In addition, the region of the signal dominated by the skin response is automatically identified. These key enhancements provide the flexibility needed to apply the algorithm successfully to 3D models illuminated by various antennas. Furthermore, applying the technique to experimental data from phantoms and a patient, as well as simulated 3D data, represents a first in the literature to the best of our knowledge. In Section 2, the algorithms used to select antennas in the neighborhood of a target antenna and estimate the skin response are described. In Section 3, the breast models used to test the algorithms are described and the results from simulated data are reported. Section 4 presents the results of the algorithm applied to measured and simulated data collected from an artificial breast model, as well as a patient scan. Section 5 concludes the paper.

## 2. METHODS

The proposed skin subtraction method estimates the skin response of the target antenna as a filtered combination of the skin reflections measured at a set of antennas:

$$\vec{r}_\tau[n] = \vec{s}_\tau[n] - \vec{q}^T \vec{b}_{\text{patch},\tau}[n] \quad (1)$$

where  $\vec{s}_\tau[n]$  is the response at target antenna  $\tau$  at time  $n$ ,  $\vec{q}$  is the vector of filter weights and  $\vec{b}_{\text{patch},\tau}[n]$  is the input vector, which consists of responses at recorded at neighboring antennas. The residual,  $\vec{r}_\tau[n]$ , is the target signal with the estimate of the skin response removed. Using adaptive filtering principles and following [2], the filter weights are computed such that the mean square error between the target signal and the estimate is minimized over the portion of the signal dominated by the skin reflection (skin dominant window or SDW).

Challenges in application to data sets collected from 3D models include defining the input vector appropriately, as well as calculating filter weights efficiently. With 3D models, the shape of the breast varies, resulting in changes in the skin reflection. The antennas may be scanned in various patterns to collect data, and different antennas may be used in different systems or versions of a system. We aim to develop an algorithm that adapts to differences in skin reflections over the breast, and is flexible enough to accommodate different scan patterns and antennas. Therefore, three critical enhancements to the 2D algorithm reported in [2] are introduced. The first addition is an automated method to define the SDW as described in Section 2.1. By defining the SDW based on signal characteristics instead of residuals as in [2], the actual skin response drives the filter weight computation. This also permits effective reduction of skin reflections that vary over the breast without user intervention to set window parameters, as well as straight-forward adaptation to different antennas that may be used to collect data.

The second enhancement is described in Section 2.2, where a method to define the antennas contributing to the input vector is introduced. Specifically, the antennas used in the estimation of a given target signal are selected such that similar regions of the model are illuminated, resulting in a physically relevant 3D neighborhood. This approach is easily adapted to different scan patterns used to collect data as well as different antennas. Finally, calculating the filter weights involves inversion of a matrix. To maintain flexibility, an automated approach is included in the approximation of the inverse matrix. The overall flow of the algorithm is shown in Figure 1.

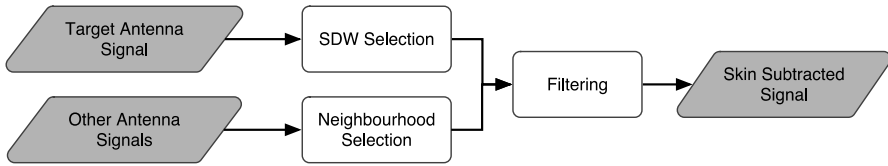


**Figure 1.** Flow chart showing the steps in the skin subtraction algorithm.

### 2.1. Skin Dominant Window Selection

As in [2], the filter weights for a given target signal are established using time averages of the statistics of a set of reflections over the window that contains the dominant skin reflection:

$$\vec{q} = \arg \min_q \sum_{n=w_1}^{w_2} \left| \vec{s}_\tau[n] - \vec{q}^T \vec{b}_{\text{patch},\tau}[n] \right|^2 \quad (2)$$

where  $w_1$  and  $w_2$  define the window. To enable application to 3D data sets, we define the SDW based on the characteristics of the signal rather than minimization of the residual. Specifically, the boundaries of this window are selected such that the significant local maxima (peaks) and minima (troughs) of the skin response are included within the SDW. An example of a signal with the SDW indicated is presented in Figure 2.

The significant local maxima and minima are established by inspecting the first and second order derivatives of the squared signal of interest. The portion of the signal at time step  $n$  is deemed to be at a maximum or a minimum if the estimate of the first order derivative is approximately equal to zero. Maxima are delineated from the minima using the second derivatives, where the maxima have a negative second derivative. As the signals are discretized, the derivatives are approximated using differences.

The significant local maxima are established using two criteria. First, the amplitude of a given peak is normalized to the maximum value of the signal. The normalized value is compared to a threshold to determine whether the peak is considered to be a local maximum. The threshold is based on the characteristics of the particular antenna, which are assumed known via simulations or measurements of thin dielectric layers similar to the skin. Next, significant peaks are only accepted if they are adjacent to another significant peak with the exception of the first and last detected significant peaks. These stipulations are designed to ensure that the detected significant peaks are in fact associated with the skin response. The first edge of the

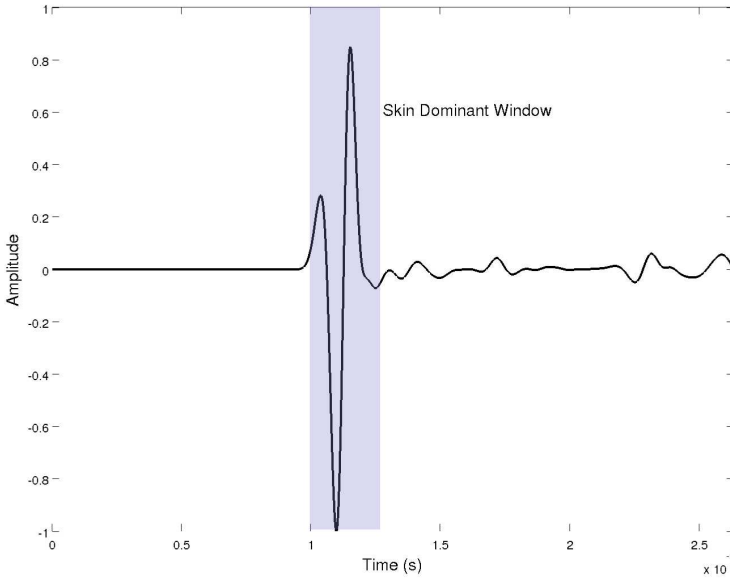


**Figure 2.** Example of a typical signal with the skin dominant window highlighted.

SDW ( $w_1$ ) is set to be the time step associated with the trough that precedes the first significant peak while the following boundary ( $w_2$ ) is the trough that follows that last significant peak. We note that this approach may be modified to suit various excitation signals and antennas.

## 2.2. Neighborhood Selection

The filter is applied to an input vector which is denoted as  $\vec{b}_{\text{patch},\tau}[n]$  for antenna  $\tau$  at time step  $n$ . This vector is defined using concatenated segments of the signals recorded at its neighboring antennas. In [2], all of the antennas in the scan are included in the neighborhood, but this does not provide reasonable results in a 3D system. Several Neighborhood selection schemes were tested, encompassing a variety of antenna distributions and potential cross correlation thresholds (e.g., [12]). The best of the tested selection schemes identifies the neighbors based on antenna proximity and the cross-correlation between the recorded signals.

The proximity criterion is evaluated using the half-energy

beamwidth (HEB) of the target antenna. The half-energy beamwidth is calculated by considering the energy on a plane perpendicular to the antenna aperture and identifying the region over which the energy is greater than half of the maximum value [13]. Antennas are defined as members of the same neighborhood if the candidate antenna and the target antenna are separated by less than twice the horizontal HEB ( $HEB_h$ ) in the horizontal direction. The antennas must also be separated in the vertical direction by less than the vertical HEB ( $HEB_v$ ) minus 1 cm. These criteria allow for selection of neighboring antennas from a 3D array of candidates, which is novel to this work. The differences in vertical and horizontal directions relate to the curvature of the breast, which is expected to vary more significantly in the vertical direction, as well as the beam of the antenna, which is asymmetric in the horizontal and vertical directions for the designs considered here. Using the maximum separation distances in the horizontal and vertical directions, a patch may be defined to describe the region in which neighboring antennas are located.

The cross-correlation is computed between the reflections recorded at a target antenna  $\tau$  and an antenna  $v$  that is a candidate for inclusion in the neighborhood. A threshold for the cross-correlation value ensures that antennas included in the neighborhood have similar responses to the target signal.

The neighborhood selection scheme is described mathematically as follows. Given that target antenna  $\tau$  is located at  $x_\tau, y_\tau, z_\tau$ , antenna  $v$  is a member of the target antenna's neighborhood ( $N_{\text{patch},\tau}$ ) if it meets the following conditions:

$$\begin{aligned}
 v \in N_{\text{patch},\tau} \quad & \text{iff} \\
 2HEB_h & \geq \sqrt{(x_\tau - x_v)^2 + (y_\tau - y_v)^2} \\
 (HEB_v - 1 \text{ cm}) & \geq \sqrt{(z_\tau - z_v)^2} \\
 \varphi & \leq \text{xcorr}(\vec{s}_\tau, \vec{s}_v)
 \end{aligned} \tag{3}$$

where  $x_v, y_v, z_v$  are the coordinates of a potential neighboring antenna,  $\varphi$  is the predetermined cross correlation threshold and  $\vec{s}_\tau$  and  $\vec{s}_v$  are the entire signals acquired at the target antenna and a potential neighbor, respectively.

### 2.3. Skin Subtraction

After determining the neighboring antennas and the boundaries of the target signal's SDW, the input vector for a given time step can be established. This is accomplished by concatenating a small segment of data from each neighboring signal within the SDW using a small window to dictate the length of the segments. This input

vector is used to estimate the skin response, which is then subtracted from the target signal. This is accomplished by filtering the input vector and determining the filter coefficients involves time-averaging of the statistics of the input vector as the small window slides across the SDW. Consequently, the skin response at a given time step is approximated as an averaged weighted combination of the data observed within the SDW at the neighboring antennas. This procedure is described in detail in the following section.

The contribution of a neighboring antenna  $v$  to the input vector at time step  $n$  is:

$$\vec{b}_v[n] = [\vec{s}_v[n - J] \dots \vec{s}_v[n] \dots \vec{s}_v[n + J]]^T \quad (4)$$

where  $2J + 1$  is the width of the small sliding window used to create the input vector [2]. Consequently, the input vector  $\vec{b}_{\text{patch},\tau}[n]$  at time step  $n$  for target antenna  $\tau$  is a column vector with contributions from each antenna in the neighborhood:

$$\vec{b}_{\text{patch},\tau}[n] = [\vec{b}_1[n]^T \dots \vec{b}_v[n]^T \dots \vec{b}_{NS}[n]^T]^T \quad (5)$$

where  $NS$  is the number of antennas accepted into the neighborhood. Once the input vector is established, the filter weights are computed such that the following cost function is satisfied

$$\vec{q} = \arg \min_q \sum_{n=w_1}^{w_2} \left| \vec{s}_\tau[n] - \vec{q}^T \vec{b}_{\text{patch},\tau}[n] \right|^2 \quad (6)$$

where  $\vec{q}$  is a column vector of filter weights, while  $w_1$  and  $w_2$  are the first and second boundaries of the SDW [2].

The normal equation:

$$\mathbf{R}\vec{q} = \vec{p} \quad (7)$$

is used to solve the minimization problem stated in (6), where  $\mathbf{R}$  is the autocorrelation matrix of the input vector, and  $\vec{p}$  is the cross correlation vector between the target signal and the input vector [8]. These values are computed using a time average over the SDW as follows:

$$\mathbf{R} = \frac{1}{m} \sum_{n=w_1}^{w_2} \vec{b}_{\text{patch},\tau}[n] (\vec{b}_{\text{patch},\tau}[n])^T \quad (8)$$

$$\vec{p} = \frac{1}{m} \sum_{n=w_1}^{w_2} \vec{b}_{\text{patch},\tau}[n] (\vec{s}_\tau[n])^T \quad (9)$$

where  $m$  is the length of the SDW. In order to calculate the filter weights, the matrix  $\mathbf{R}$  must be inverted. This is a challenge, as this matrix is ill-conditioned as a result of the high degree of similarity

between the neighboring signals over the SDW [2]. Consequently, the autocorrelation matrix is replaced with a low rank approximation. The generalized cross validation (GCV) method is used to estimate the rank of  $\mathbf{R}$  [9]. This technique starts by applying eigenvalue decomposition to the autocorrelation matrix as shown,

$$\mathbf{R} = \mathbf{U}\mathbf{\Lambda}^{-1}\mathbf{U} \quad (10)$$

where  $\mathbf{\Lambda}$  is a diagonal matrix of eigenvalues and  $\mathbf{U}$  is a matrix of corresponding eigenvectors. The GCV approximates the rank to be the value that minimizes the following function:

$$g(k) = \frac{\|(\mathbf{I} - \mathbf{R}\mathbf{R}^{-1}(k)\vec{p})\|^2}{|\text{trace}(\mathbf{I} - \mathbf{R}\mathbf{R}^{-1})|} \quad (11)$$

where  $\mathbf{I}$  is the identity matrix and  $\mathbf{R}^{-1}(k)$  is the inverse of the low rank approximation of  $\mathbf{R}$  for any given  $k$ .

The filter weights are thereby computed as:

$$\vec{q}^T = (\mathbf{R}_{\text{GCV}})^{-1}\vec{p} \quad (12)$$

where  $(\mathbf{R}_{\text{GCV}})^{-1}$  is the inverse of the low rank approximation of  $\mathbf{R}$  as calculated by the GCV method. The filter is applied to the entire duration of the target signal, using the same procedure as described above to establish the input vector [2]. Consequently, the final skin-subtracted signal using the proposed method is represented by:

$$\vec{r}_\tau[n] = \vec{s}_\tau[n] - \vec{q}^T \vec{b}_{\text{patch},\tau}[n] \quad (13)$$

We note that at least 9 antennas are required to be in a neighborhood such that the filter coefficients are computed effectively. Signals collected at antennas without 9 neighbors do not have the skin reflection reduced and are not included in further processing.

#### 2.4. Performance Measures

The skin subtraction technique's ability to reduce the dominant response is quantified using several different measures. The reduction of the skin response is important; however, the preservation of the tumor response must also be considered. To assist in this assessment, simulations are performed with and without the tumor present in a given model. This permits isolation of the tumor response by taking the difference between the two sets of simulations, giving the tumor response at time step  $n$  as:

$$\vec{t}_\tau[n] = \vec{s}_\tau[n] - \vec{s}_{nt,\tau}[n] \quad (14)$$

where  $\vec{s}_{nt,\tau}[n]$  is the reflection recorded at antenna  $\tau$  without the tumor present.

Several different metrics are used to compare signals before and after the algorithm is applied, and the mean and standard deviation of the metrics for groups of antennas are calculated.

To assess the reduction of the skin reflection, the **skin subtraction ratio (SSR)** is calculated. Specifically, the peak-to-peak (PP) values of the segment of the signal within the SDW after and before skin subtraction are compared:

$$\text{SSR}_\tau = 20 \log \left( \frac{\max_{n \in \text{SDW}} \vec{r}_\tau[n] - \min_{n \in \text{SDW}} \vec{r}_\tau[n]}{\max_{n \in \text{SDW}} \vec{s}_\tau[n] - \min_{n \in \text{SDW}} \vec{s}_\tau[n]} \right) \quad (15)$$

To give a sense of the response of the tumor relative to the skin, the **tumor-to-skin ratio (TSR)** compares the PP value of the tumor response only and the PP value of the signal over the SDW. Specifically,

$$\text{TSR}_\tau = 20 \log \left( \frac{\max(\vec{t}_\tau) - \min(\vec{t}_\tau)}{\max_{n \in \text{SDW}} \vec{s}_\tau[n] - \min_{n \in \text{SDW}} \vec{s}_\tau[n]} \right) \quad (16)$$

This metric may be computed prior to or following skin subtraction. For calculation following skin subtraction, the data sets collected with and without the tumor present are processed to remove the skin response, then the tumor response is isolated by taking the difference between these processed data sets.

To provide insight into the changes in the tumor response after filtering, the **tumor-to-tumor ratio (TTR)** compares the PP values of the tumor response before and after skin subtraction.

The SSR, TSR and TTR are calculated at each antenna, resulting in a significant amount of data. The mean and standard deviation of these results are computed over each row to assist in visualizing results.

For measured data, tumor-free responses are not typically available. The efficacy of the algorithms is demonstrated by examining the skin suppression (SSR) and by forming images. The detection of a tumor in an image is quantified by calculating the **signal-to-clutter ratio (SCR)**, which compares the maximum response associated with the tumor to the maximum response in the rest of the image. With phantoms, the location of the tumor is typically known. For our patient study, mammograms and magnetic resonance images of the breast are available; these images are analyzed to by radiologists in order to identify the region of the breast in which a tumor response is expected in the microwave image.

### 3. INITIAL TESTING WITH SIMULATED DATA

The algorithm is first tested with simulated data generated with realistically shaped models to gain insight into its efficacy. A series of increasingly complex models are tested to assess sensitivity to interior property distributions, as well as robustness to different shapes and sensors.

#### 3.1. Models

The models used to test the skin subtraction algorithm are derived from Magnetic Resonance (MR) images of the breast collected from volunteers (study #18463 as approved by the University of Calgary Conjoint Health Ethics Research Board). The MR voxel intensities are converted to dielectric property values using the procedure outlined in [14, 15].

Five different models are examined in this paper in order to test the algorithm in a variety of scenarios. Models A to C are based on the same MR scan, with increasing levels of complexity incorporated. Model A has homogeneous tissue in the interior and constant skin thickness. Models B and C include variations in the distribution of the tissues in the breast interior. Model C also includes non-uniform skin thickness and properties.

To test robustness to different breast shapes, Models D and E are developed from different breast MR scans than Models A–C. The characteristics of these models are summarized in Table 1, while Figure 3(a) shows a cross-section through Model A at the center of the

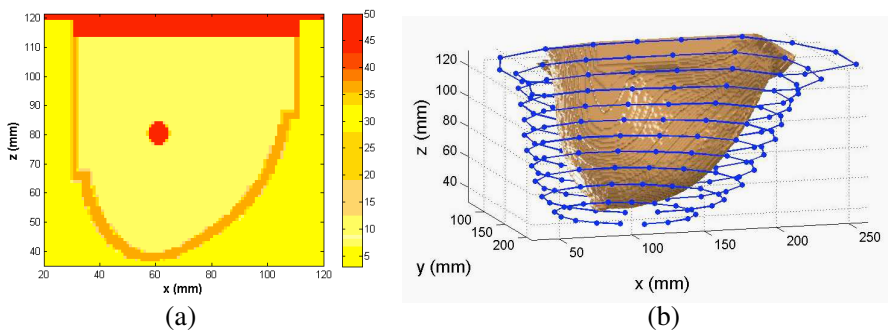


**Figure 3.** (a) Cross-section of Model A at the plane that intersects with the center of the tumor. The color bar indicates the relative permittivity of the model. (b) 3D rendering of the skin surface and antenna scan pattern.

**Table 1.** Simulation models. All models except C have uniform skin thickness (2 mm) and properties ( $\epsilon_r = 36$ ,  $\sigma = 4$ ).

Model	Antenna	MRI	Pixel Intensity Mapping Details
A	Dipole	1	Breast interior mapped as homogeneous fatty tissue ( $\epsilon_r = 9$ , $\sigma = 0.4$ )
B	Dipole	1	Breast interior segmented and mapped as fatty ( $\epsilon_r = 9$ , $\sigma = 0.4$ ) or glandular tissues ( $\epsilon_r = 16$ , $\sigma = 1$ )
C	Dipole	1	Entire breast linearly mapped resulting in varying properties for all tissues ( $\epsilon_r = 1-36$ , $\sigma = 0.4-4$ )
D	Dipole	2	Breast interior mapped as homogeneous fatty tissue ( $\epsilon_r = 9$ , $\sigma = 0.4$ )
E	BAVA	3	Breast interior mapped as homogeneous fatty tissue ( $\epsilon_r = 8.19$ , $\sigma = 0.4$ )

tumor. While the maximum values representing glandular tissues are lower than expected from [16], the models are designed to demonstrate the performance of the algorithm in increasingly complex scenarios. Models A–C and E contain 6-mm diameter tumors, while Model D contains an 8-mm diameter tumor. Each of the models is created with and without a tumor inserted in order to permit the tumor reflection to be isolated by simply subtracting the appropriate signals.

Simulations of the models are performed with an in-house finite difference time domain (FDTD) method code (Models A–D) or a commercial FDTD code (SEMCAD, SPEAG, Zurich). Each model is illuminated with an antenna that is positioned at various locations around the breast. To demonstrate that the algorithm may be adapted to different antennas, two antennas are used in simulations. Models A–D are illuminated with a Wu-King resistively loaded dipole antenna [17], while Model E is illuminated with a balanced antipodal Vivaldi antenna (BAVA) [13]. Both antennas are excited with a differentiated Gaussian pulse with a full-width half-maximum bandwidth from 1.3–7.6 GHz and a center frequency of 4 GHz. For the definition of the patch used in the neighborhood selection algorithm, the HEB for the dipole is  $44 \times 35$  mm and the HEB for the BAVA is  $34 \times 45$  mm.

The breast models are scanned by repositioning the antenna

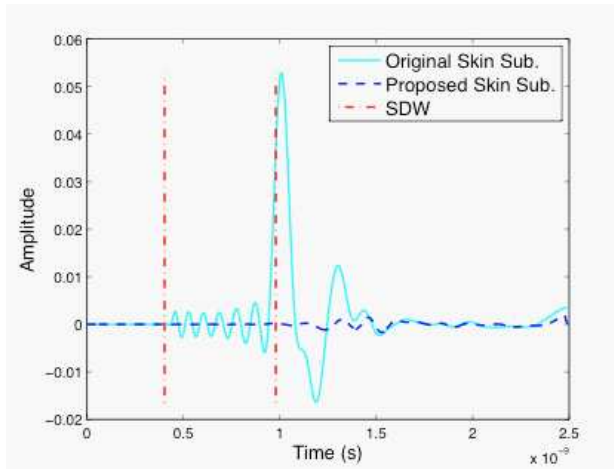
around the breast model. In the system under development at the University of Calgary [4], the woman lies prone with the breast extending into a tank of immersion liquid. At a selected elevation ( $z = \text{constant}$ ), a single antenna is scanned around the breast model (i.e., in the  $x$ - $y$  plane). At one elevation, the antenna locations at which data are recorded are referred to as a row. For models A–C, an elliptical scanning pattern is used in the  $x$ - $y$  plane to position the antenna in order to follow the breast shape while maintaining approximately 2 cm separation between the antenna and breast. The elliptical scanning pattern is repeated at 9 elevations separated by 1 cm. A 3D depiction of the scan pattern is shown in Figure 3(b). At each elevation, the breast model has different cross-sectional areas, resulting in a different number of antennas in each row. This leads to a scan consisting of 245 antenna locations placed in 9 rows with up to 32 antennas per row. Model D also has a scan pattern consisting of 245 antennas arranged in 9 rows separated by 1 cm. For Model E, the elliptical scan pattern consists of 11 rows of 16 antennas. Again, the antenna aperture is located approximately 2 cm away from the breast model.

### 3.2. Results

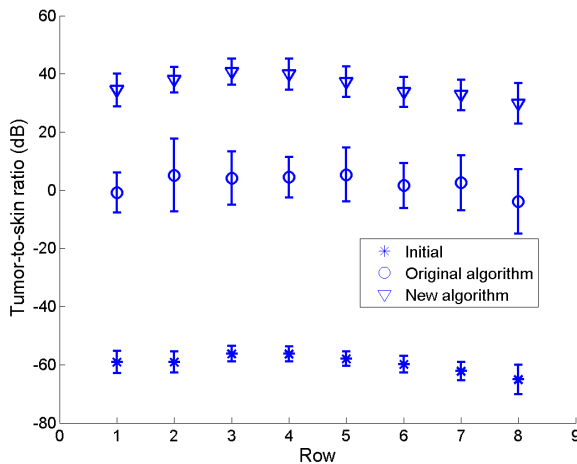
The proposed algorithm and the skin reduction technique reported in [2] are compared by applying both algorithms to Model A. To make an objective evaluation while remaining as consistent as possible with the procedure outlined in [2], the small sliding windows are the same size for both trials ( $J = 3$ ).

Figure 4 shows an example of the results when both skin subtraction algorithms are applied to a selected signal. For the original skin subtraction approach described in [2], all reflected signals are used to approximate the target signal. With the modified approach, the signals used in the approximation are defined with the neighborhood selection approach discussed above. The importance of the neighborhood selection is illustrated in Figure 4, as the skin response found within the SDW is more effectively removed using the proposed algorithm. This result was consistently observed for the 245 antennas; the average skin subtraction ratio over all antennas is 62.2 dB for the original algorithm, while the average of this metric improves substantially to a value of 91.9 dB when the proposed technique is applied.

To gain further insight into the algorithm's ability to subdue the skin response and to ensure that the residual skin reflection does not dwarf the tumor response, the tumor-to-skin ratio of Model A is examined before and after skin subtraction. Figure 5 demonstrates the resulting tumor-to-skin ratios. The ratios observed prior to



**Figure 4.** Comparison of the resulting skin subtracted signal when both algorithms are tested on the same signal. The proposed algorithm generates improved results as the dominant skin reflection is more effectively suppressed.



**Figure 5.** Tumor-to-skin ratios (TSR) before and after applying both skin subtraction techniques to Model A. As the number of signals recorded within a given data set is substantial (245), the resulting tumor-to-skin ratios are shown as the average and standard deviation of the ratio over every row.

skin subtraction lie at about  $-65$  dB, while the proposed algorithm generates ratios of approximately  $35$  dB. The technique reported in [2] does not sufficiently suppress the dominant skin response as its average tumor-to-skin ratio is  $0$  dB, indicating that the residual skin response has the same PP value as the tumor response.

The algorithm is further tested by applying it to models that include glandular tissue distributions. Figure 6 summarizes the skin subtraction ratios obtained when Models A, B and C are tested. The ratios are similar for all three models, demonstrating that the skin subtraction process is successful. It is also important to note that, although Model C exhibits variations in the thickness and dielectric properties of the skin, the performance of the algorithm does not degrade. The tumor-to-skin ratios are also examined for these models, indicating that this ratio degrades for Models B and C, as expected. However, the average response remains above  $0$  dB for all cases.

To assess whether the proposed algorithm is capable of adapting to breast models of different shapes and sizes, the skin subtracted signals from Models A and D are compared in Figure 7. In both cases, the skin response is effectively removed. The values for Model D are consistent with the values for Model A as the average skin subtraction ratios differ by only  $6$  dB at most. On average, the dominant skin response is subdued by  $96$  dB, demonstrating that the algorithm is robust to models of varying shapes and sizes.

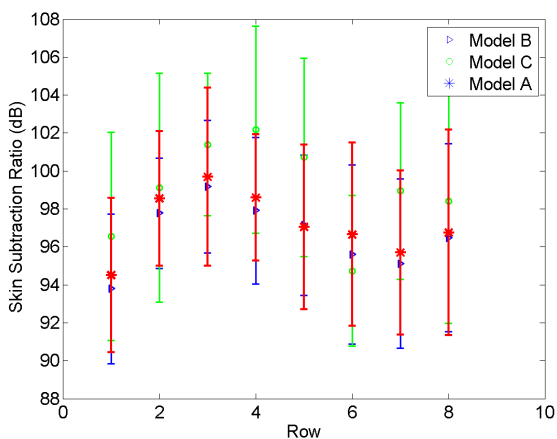


**Figure 6.** Summary of the skin subtraction ratios (SSR) calculated from models with the same geometry but different interior property distributions.

Finally, the algorithm is tested on signals recorded using two different antennas and two different models (D and E). Example of an original signal and the resulting skin subtracted signal are shown in Figure 8 for both antennas, along with the corresponding SDWs. The

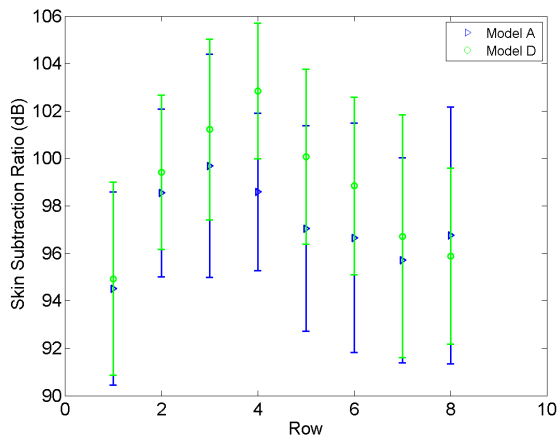


**Figure 7.** Summary of the skin subtraction ratios (SSR) calculated from models with the same interior property distribution but different geometries.

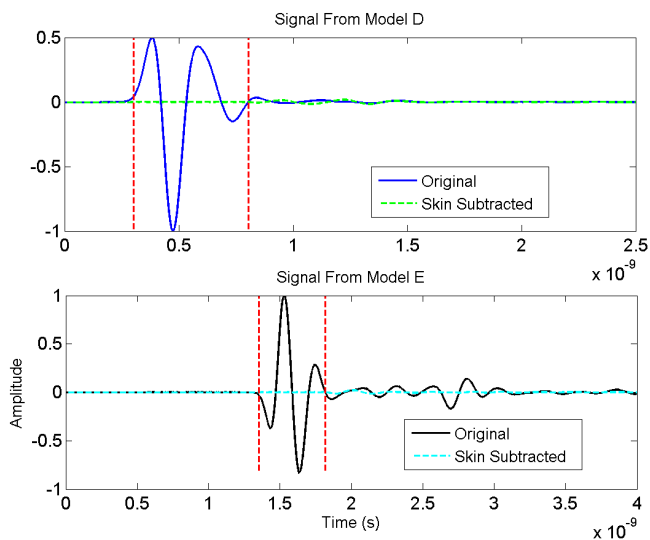


**Figure 8.** Comparison of the signals recorded from two different models, using two different antennas before and after skin subtraction.

adaptive nature of the SDW selection process is clearly illustrated, as the shape of the original signal for both cases is significantly different. The skin response in both cases has also been successfully subdued, as responses are not evident within the SDW. It is also interesting to note that the skin subtraction algorithm also reduces the secondary reflection seen in Model E at approximately 2.5 ns. This property is highly desirable as this response is likely a secondary skin reflection caused by multiple reflections that occur within the antenna. The average overall skin subtraction ratios for both models are 98.79 dB and 99.33 dB, respectively, indicating that the algorithm's performance is independent of the sensor used.

#### 4. TESTING WITH PHANTOM AND PATIENT DATA

The proposed algorithm has proven robust with 3D models and simulated data. To test the algorithm on measured data, a prototype system developed at the University of Calgary is employed. Two test cases are considered: a phantom (model) with known properties and an inclusion, and a patient scan. Simulations are also performed of the phantom to permit comparison of measured and simulated data.

##### 4.1. Prototype System

A prototype microwave imaging system has been developed for monostatic, radar-based data collection at the University of Calgary [4]. The prototype is called the Tissue Sensing Adaptive Radar (TSAR) system. The woman to be scanned lies on an examination table on her stomach with one breast extending through the hole in the table top. Under the table, a tank of immersion liquid (canola oil) contains several sensors. A photo of the tank and antenna is shown in Figure 9(a), while Figure 9(b) depicts the orientation of a patient in the TSAR system. The sensors include an ultra-wideband antenna for transmitting and receiving signals, a laser that is used to obtain an estimate of the surface of the object under test, and a digital camera that is used to monitor the scan. The antenna and laser are attached to an arm that moves vertically. The entire tank also rotates. Therefore, the antenna is scanned in a cylindrical pattern around the breast. The scan pattern is designed based on the extent of the object or breast into the tank, which is typically evaluated via images collected by the digital camera.

The antenna that is used in the prototype system is a BAVA-D (balanced antipodal Vivaldi antenna with director) [13]. The director is a piece of material with higher dielectric constant that is

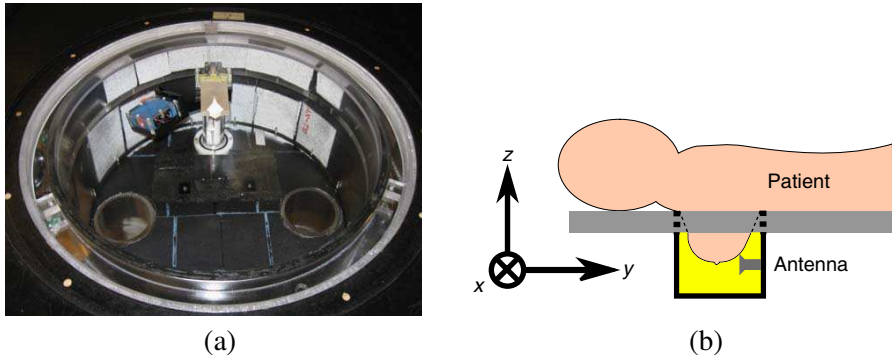


**Figure 9.** (a) Photo of the TSAR Immersion tank (empty of immersion medium), antenna, and laser. (b) Orientation of a patient in the TSAR system.

placed in the antenna aperture in order to narrow the beam of the antenna in the near field. The HEB of this antenna is  $23$  (vertical)  $\times$   $42$  (horizontal) mm.

#### 4.2. Breast Model

For an initial test of the proposed algorithm on measured data, a simple model is used [18]. This model is manufactured from a dielectric material with relative permittivity of 15 and loss tangent less than 0.002 (Eccostock HiK, Emerson and Cumming Microwave Products, Randolph, MA). The model consists of a series of discs that are connected with a rod to form the phantom. The shape of the phantom may be described as a hemisphere of radius 5 cm connected to a cylinder of diameter 10 cm. A region representing the nipple is also included on the surface of the hemisphere. The breast model is placed in the hole in the top of the prototype and extends into the immersion medium of oil. While the model does not include a skin layer, the differences between the electromagnetic properties of the dielectric material and oil gives rise to a significant reflection. To mimic a tumor, a Teflon inclusion of 7.9 mm diameter and 19.4 mm length is placed at a radial distance of 25 mm from the center of the model.

To scan the model, the antenna is moved (with motors integrated into the prototype) to 7 elevations separated by 1 cm. Reflections are collected at 20 locations per row and the rows are rotationally offset by 3 degrees. The reflections are recorded with a vector network analyzer (VNA) (8722ES, Agilent Technologies, Palo Alto, CA) over 1601 points covering the range from 50 MHz to 15 GHz. These measured reflections

are then weighted with a differentiated Gaussian signal to obtain the same waveform as transmitted during simulation, then transformed into the time domain [18]. We note that the FWHM bandwidth of the differentiated Gaussian signal (1.3–7.6 GHz) requires an expanded measurement range in order to effectively synthesize the time-domain signal of interest without introducing significant artifacts.

For comparison, simulations of the breast model illuminated by the BAVA-D antenna are also performed. The simulations are described in detail in [4] and include key features such as the tank and the tank lid. The antenna in simulations is excited with the same differentiated Gaussian pulse as synthesized with measured data. Comparison of simulations and measurements demonstrates good agreement, particularly between the dominant reflections [4]. Finally, simulations are performed with and without the inclusion present in the model in order to permit isolation of the response from this object.

The skin subtraction algorithm is first applied to simulated data. Figure 10 compares tumor-to-skin ratios before and after the algorithm is applied, demonstrating that the reflection from the oil/dielectric interface is effectively reduced. The tumor response is isolated by taking the difference between simulations performed with and without the tumor present, and the PP values are compared before and after skin subtraction. Figure 10 also demonstrates that the tumor reflection is reduced by the algorithm, but nonetheless is greater than the skin response after the algorithm is applied.

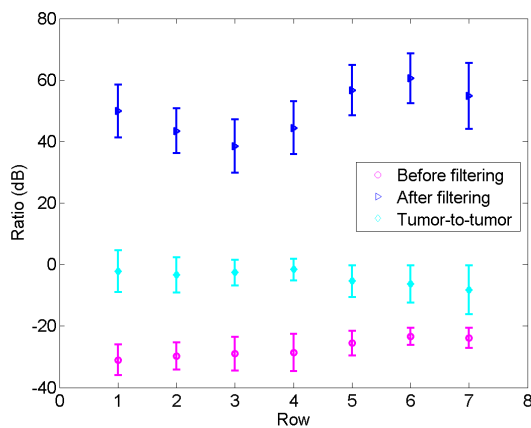


**Figure 10.** Tumor-to-skin response (TSR) before and after filtering. The tumor-to-tumor ratio (TTR) is also shown, indicating that some degradation occurs.

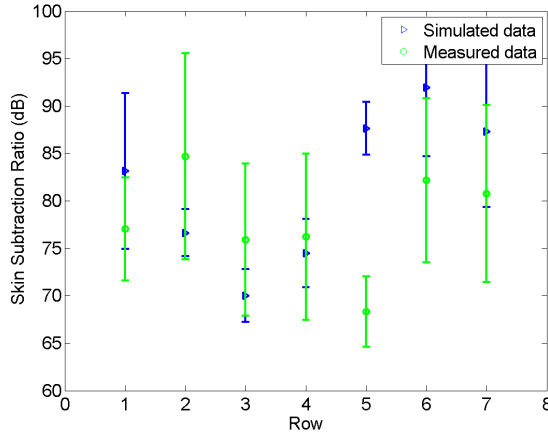


**Figure 11.** Skin subtraction ratio (SSR) for simulated and measured data.

The reduction of the dominant reflection is compared for simulated and measured data in Figure 11. For both types of data, the algorithm reduces the skin reflection significantly. The performance is similar; however, some rows show greater reduction of the reflection in simulated data while others show greater reduction in measured data. Further investigation revealed that, for a selected target antenna, the same antennas are selected to approximate the skin response. For the hemispherical model, simulated data collected at a row of antennas contains reflections that are almost identical, while measured data shows more variation. At some antennas, this variation results in degraded performance of the algorithm, while it is advantageous at others.

Figure 12 shows images of the hemispherical phantom that are created with the TSAR algorithm [18]. After the skin subtraction algorithm is applied, the data are focused to create a 3D image by a simple time-shift and sum approach. The estimate of the surface obtained with the laser is included in order to more accurately calculate travel times through the immersion liquid and model. The results in Figure 12 illustrate that the TSAR imaging algorithm permits detection and localization of the inclusion. These images are normalized to the maximum response, as the non-tomographic radar system aims to identify significant scattering objects instead of reconstruct material properties. The SCR for simulated data is 13.2 dB, while the SCR for measured data is 10.75 dB. This is consistent

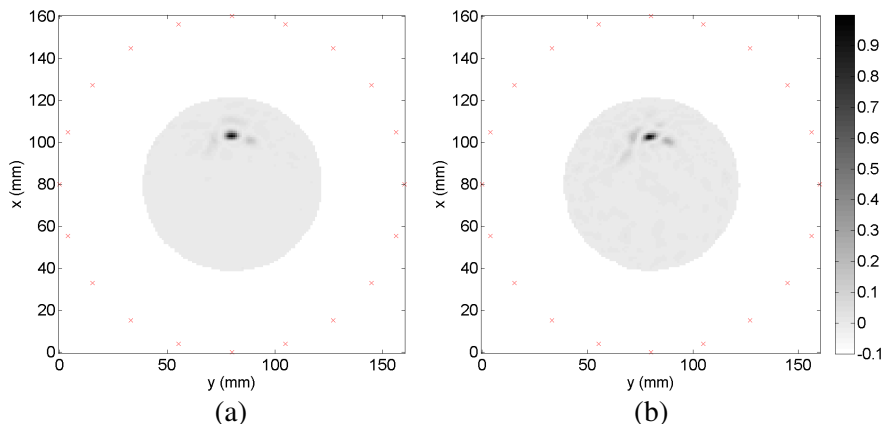


**Figure 12.** TSAR images of the plane cutting through the phantom at the location of the tumor and parallel to the end of the cylinder created with (a) simulated data and (b) measured data. Both images are normalized to the maximum responses.

with the increased clutter expected with measured data, and this increased clutter may also be observed in Figure 12. Therefore, both cases demonstrate that the reflection from the oil/dielectric interface is reduced such that the inclusion is easily detected in images.

Figure 13(a) shows an example of reconstructing TSAR data without suppressing the skin response. While the maximum response in Figure 13(a) is only 4 times larger than the tumor response of Figure 12(b), the tumor response is not visible in the image without skin subtraction. The secondary response noted in Figure 8(b) results in the dominant response in the center of the image. The skin subtraction algorithm filters the entire signal, reducing this secondary skin response and permitting detection of the inclusion. This illustrates the need for a comprehensive skin subtraction algorithm.

Figure 13(b) shows a reconstruction of the data with the previous skin subtraction algorithm applied [6]. While the tumor is clearly detected in this simple model, increased spreading of the response is observed. It is anticipated that the Woody algorithm would not suffice with more complex data sets that involve greater variations in the skin responses. In particular, the Woody algorithm operates on a row-by-row basis, leading to good results with the circular cross-section of the model but unable to account for the variability of patient data.

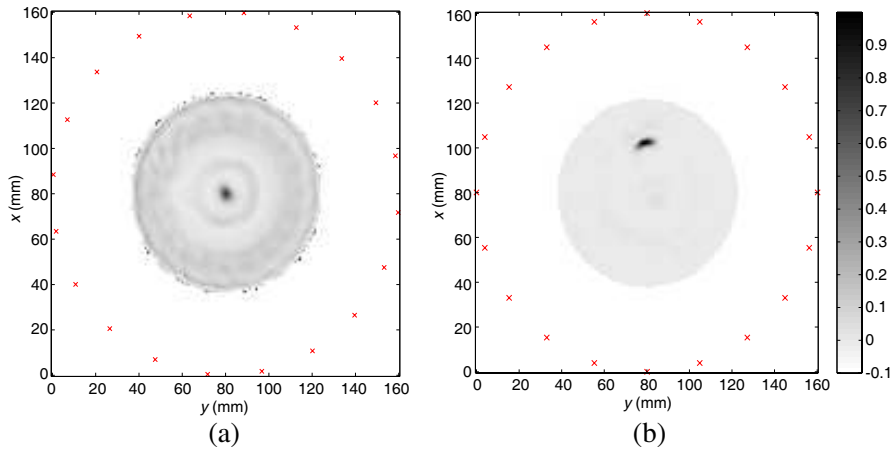


**Figure 13.** Cross section of TSAR image of measured data (Figure 12(b)) without any skin subtraction. (a) and with the original Woody skin subtraction technique.

### 4.3. Sample Patient Data

The prototype system has been tested on 3 volunteers and 9 patients (Studies #21859 and #22121 as approved by the University of Calgary Conjoint Health Research Ethics Board). To demonstrate the efficacy of the skin subtraction algorithm, we present one case in detail. This patient had a 10 mm diameter mass at the 4 o'clock radian of the right breast. This mass was observed with mammography, ultrasound and magnetic resonance imaging. Clinical images also classified the breast tissue as heterogeneous. Biopsy and post-surgical pathology indicated that the lesion was grade II/III metaplastic carcinoma. The TSAR scan of the patient's right breast involved collecting microwave measurements at 6 rows separated by 1 cm with 30 antenna locations per row, resulting in 180 antenna locations in total. Laser measurements were also collected and used to estimate the breast surface [19].

To create images, the neighborhood-based skin subtraction algorithm is applied first. As with the hemispherical model, the data are focused with a simple time-shift and sum approach to create a 3D image. The patient-specific laser surface estimate is incorporated into calculation of travel times between sensors and focal points, specifically to determine path-dependent distances in oil and breast tissue. The TSAR image through the maximum response is shown in Figure 14, along with an image extracted from the breast MR scan. The TSAR

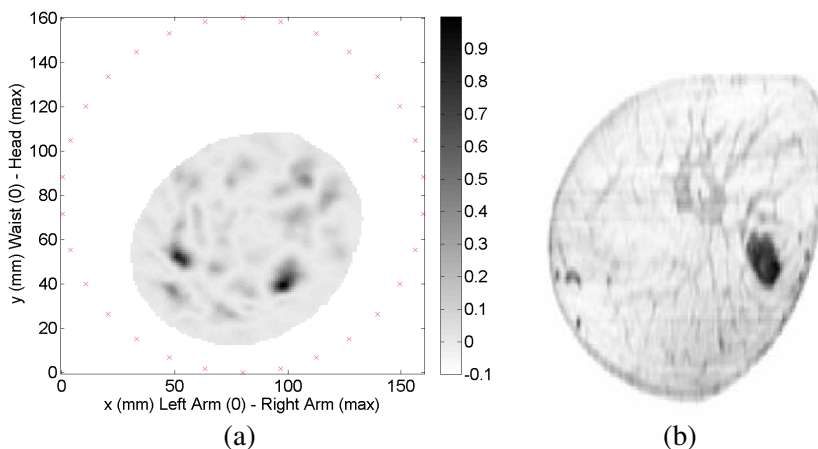


**Figure 14.** (a) TSAR image of a patient with a known 1 cm lesion at 4 o'clock. (b) Slice extracted from contrast-enhanced MR image of the same patient.

image illustrates a response at 4 o'clock, which is in agreement with the known location of the tumor. The other responses in the image correspond to clutter, perhaps originating from the glandular tissues. This compelling result suggests that the neighborhood-based skin subtraction algorithm is capable of effectively reducing skin reflections in measured data from patients.

## 5. CONCLUSION

This paper presents a skin subtraction algorithm that fuses a neighborhood selection technique with an enhanced version of a previously proposed method to reduce the skin response. The neighborhood selection technique establishes the input data to the enhanced skin reduction method based on the proximity of the antennas to one another and the normalized cross-correlation between recorded signals. This permits selection of antennas from a collection of antennas positioned in 3D space, therefore extending the algorithm to 3D applications.

The proposed algorithm is the first skin subtraction algorithm to successfully process signals recorded from 3D realistic breast models using a monostatic system. The algorithm also was proven to be robust to various breast geometries, tissue distributions, and the type of antenna used to acquire the data. Promising results were also

obtained when applying the algorithm to simulated and measured data collected from a phantom. Finally, application to patient data demonstrated a response in the microwave image at the location where a tumor was known to exist. Therefore, the proposed algorithm is flexible, robust and adaptable to a range of practical conditions (e.g., different sensors). Future work includes incorporating the neighborhood selection technique to improve the focusing algorithm used to create the final images of the breast.

## ACKNOWLEDGMENT

The authors wish to thank Jeff Sill for collection of simulated data and Jeremie Bourqui for collection of measured data. This work was supported by NSERC, AHFMR and UTI.

## REFERENCES

1. Li, X. and S. C. Hagness, "A confocal microwave imaging algorithm for breast cancer detection," *IEEE Microw. Wireless Comp. Lett.*, Vol. 11, 130–132, Mar. 2001.
2. Bond, E. J., et al., "Microwave imaging via space-time beamforming for early detection of breast cancer," *IEEE Trans. Ant. Propag.*, Vol. 51, 1690–1705, Aug. 2003.
3. Sill, J. M. and E. C. Fear, "Tissue sensing adaptive radar for breast cancer detection: Experimental investigation of simple tumor models," *IEEE Trans. Microw. Theory Tech.*, Vol. 53, 3312–3319, Nov. 2005.
4. Bourqui, J., et al., "A prototype system for measuring microwave frequency reflections from the breast," *Int. J. Biomed. Imag.*, Vol. 2012, 2012.
5. Klemm, M., et al., "Microwave radar-based differential breast cancer imaging: Imaging in homogeneous breast phantoms and low contrast scenarios," *IEEE Trans. Ant. Propag.*, Vol. 58, 2337–2344, 2010.
6. Fear, E. C. and J. M. Sill, "Preliminary investigations of tissue sensing adaptive radar for breast tumor detection," *Proc. 25th Ann. Int. Conf. IEEE Eng. Med. Biol. Soc.*, 3787–3790, 2003.
7. Jacobsen, S. and Y. Birkelund, "Improved resolution and reduced clutter in ultra-wideband microwave imaging using cross-correlated back projection: Experimental and numerical results," *Int. J. Biomed. Imag.*, Vol. 2010, 2010.

8. O'Halloran, M., et al., "Quasi-multistatic MIST beamforming for the early detection of breast cancer," *IEEE Trans. Biomed. Eng.*, Vol. 57, 830–840, 2010.
9. Maskooki, A., E. Gunawan, C. B. Soh, and K. S. Low, "Frequency domain skin artifact removal method for ultra-wideband breast cancer detection," *Progress In Electromagnetics Research*, Vol. 98, 299–314, 2009.
10. Wanjun, Z. and F. Chin, "Entropy-based time window for artifact removal in UWB imaging of breast cancer detection," *IEEE Signal Proc. Lett.*, Vol. 13, 585–588, 2006.
11. Winters, D. W., et al., "Estimating the breast surface using UWB microwave monostatic backscatter measurements," *IEEE Trans. Biomed. Eng.*, Vol. 55, 247–256, Jan. 2008.
12. Maklad, B. and E. C. Fear, "Reduction of skin reflections in radar-based microwave breast imaging," *Proc. 30th Ann. Int. Conf. IEEE Eng. Med. Biol. Soc.*, 21–24, 2008.
13. Bourqui, J., et al., "Balanced antipodal vivaldi antenna with dielectric director for near-field microwave imaging," *IEEE Trans. Ant. Propag.*, Vol. 58, 2318–2326, 2010.
14. Sill, J. M., et al., "Realistic breast models for second generation tissue sensing adaptive radar system," *Proc. EuCAP 2007*, 4, 2007.
15. Kurrant, D. J. and E. C. Fear, "An improved technique to predict the time-of-arrival of a tumor response in radar-based breast imaging," *IEEE Trans. Biomed. Eng.*, Vol. 56, 1200–1208, 2009.
16. Lazebnik, M., et al., "A large-scale study of the ultrawideband microwave dielectric properties of normal breast tissue obtained from reduction surgeries," *Phys. Med. Biol.*, Vol. 52, 2637–2656, 2007.
17. Sill, J. M. and E. C. Fear, "Tissue sensing adaptive radar for breast cancer detection: Study of immersion liquids," *Electron. Lett.*, Vol. 41, 113–115, 2005.
18. Fear, E. C., et al., "Antenna evaluation for ultra-wideband microwave imaging," *Int. J. Ant. Prop.*, Vol. 2010, 2010.
19. Williams, T. C., J. Bourqui, T. R. Cameron, M. Okoniewski, and E. C. Fear, "Laser surface estimation for microwave breast imaging systems," *IEEE Trans. Biomed. Eng.*, Vol. 58, 1193–1199, 2010.